Applied Catalysis B: Environmental 241 (2019) 89–94

Contents lists available at ScienceDirect

Applied Catalysis B: Environmental

journal homepage: www.elsevier.com/locate/apcatb

Hierarchical “nanoroll” like $MoS_2/Ti_3C_2T_x$ hybrid with high electrocatalytic hydrogen evolution activity

Jiapeng Liu, Yizhe Liu, Danyun Xu, Yuanzhi Zhu, Wenchao Peng, Yang Li, Fengbao Zhang, Xiaobin Fan*

School of Chemical Engineering and Technology, State Key Laboratory of Chemical Engineering, Collaborative Innovation Center of Chemical Science and Engineering, Tianjin University, Tianjin 300072, China

ARTICLE INFO

Keywords:
MoS_2
MXene
Hierarchical
Nanoroll
Hydrogen evolution reaction

ABSTRACT

Developing highly efficient noble-metal-free electrocatalysts for hydrogen evolution reaction (HER) has attracted increasing attentions. Here, we report a simple strategy to synthesize the hierarchical “nanoroll” like $MoS_2/Ti_3C_2T_x$ hybrid by combining liquid nitrogen-freezing and subsequent annealing. The quick freezing of the $Ti_3C_2T_x$ nanosheets and ammonium tetrathiomolybdate mixture causes a sudden change in the strain of $Ti_3C_2T_x$, which leads to an interesting “nanoroll” like hierarchical structure. After annealing at H_2/Ar atmosphere, vertically aligned molybdenum sulfide (MoS_2) crystallites are in situ formed in and on the nanoroll like $Ti_3C_2T_x$. Notably, this hierarchical $MoS_2/Ti_3C_2T_x$ hybrid exhibits excellent HER catalytic activity with a small onset overpotential of 30 mV, and a more than 25-fold increase in the exchange current density compared with MoS_2 was observed.

1. Introduction

Hydrogen evolution reaction (HER) is an efficient fossil fuel-free path to produce hydrogen, which is an attractive energy carrier to address the global environmental and energy crisis [1–6]. Platinum (Pt)-based catalysts show brilliant catalytic performance for HER, but the high cost and scarcity severely limit their pervasive application [7–9]. Thus, great efforts have been made to develop earth-abundant catalysts that potentially could replace Pt. Among them, molybdenum disulfide (MoS_2) is one of the most promising candidates, because its hydrogen adsorption free energy (ΔG_H) is near the optimal value of 0 eV [10–13].

The HER activity of MoS_2 is mainly derived from the edge sites, despite the possible contribution from the vacancies in the basal plane (of 1T-MoS_2, in particular) [12,14–19]. Therefore, exposing more edge sites is an effective strategy to enhance the catalytic activity of MoS_2. For example, exfoliated MoS_2 nanosheets [20–23], mesoporous MoS_2 foam [24,25] and vertically aligned MoS_2 [26–28] show significant increase in catalytic activity when compared with bulk MoS_2. The electrocatalytic performance of the MoS_2 is also determined by some kinetic factors, especially the electron transport between the MoS_2 and electrolyte [15,29]. Nevertheless, the natural 2H-MoS_2 (hexagonal structure) is a semiconductor, and the metallic 1T phase (trigonal structure) is metastable [15,21,30]. Therefore, conductive additives or supports, such as conductive carbon and graphene, are usually introduced to reduce the resistive loss and enhance the catalytic activity [5,31–35].

Two-dimensional (2D) MXenes, such as $Ti_3C_2T_x$ (T_x denotes surface functionalization, such as –O, −OH, and –F), is a new member of 2D materials [36–41]. They show distinguished characteristics from graphene, such as the combination of hydrophilic surfaces and good electrical conductivity [42–45]. Therefore, it may be used as a promising support to disperse catalysts. For example, MXenes supported Rh nanoparticles, CdS nanosheets, In_2S_3 nanoparticles, layered double hydroxide and carbon nitride catalysts have been successfully prepared and showed excellent catalytic performances in hydrodechlorination, photocatalytic and electrocatalytic oxygen evolution [46–50]. Meanwhile, MXenes has attracted much attention for HER reaction [41,51–60]. For example, the hybrid of MoS_2 and MXene showed significant improvement in HER reaction [61]. Nevertheless, the development of MXene-based hybrid system is still in a very infant stage in contrast to the prosperity of other 2D materials. And, the MXene-based hybrid with interesting hierarchical structures and excellent performance attract particular interest.

In this study, we report a simple strategy to synthesize the $MoS_2/Ti_3C_2T_x$ hybrid with an interesting “nanoroll” like hierarchical structure. Importantly, this hierarchical $MoS_2/Ti_3C_2T_x$ hybrid exhibit

* Corresponding author.
E-mail address: xiaobinfan@tju.edu.cn (X. Fan).

https://doi.org/10.1016/j.apcatb.2018.08.083
Received 14 June 2018; Received in revised form 23 August 2018; Accepted 31 August 2018
Available online 01 September 2018
0926-3373/

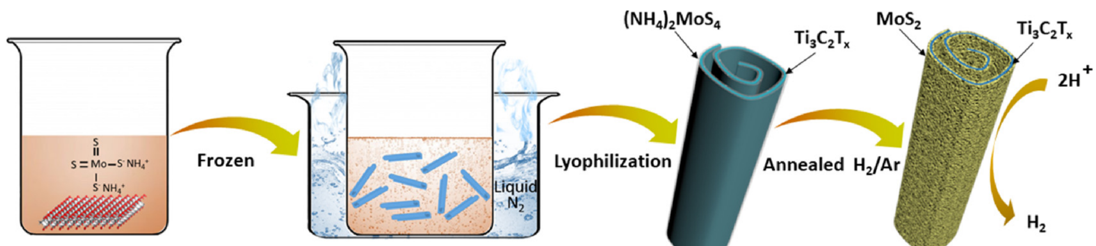

Scheme 1. Preparation of the "nanoroll" like $MoS_2/Ti_3C_2T_x$ hybrid by combining liquid nitrogen-freezing and subsequent annealing.

excellent HER catalytic activity with a small onset overpotential of 30 mV. More than 25-fold increase in the exchange current density compared with MoS_2 was observed.

2. Experimental section

2.1. Synthesis of $Ti_3C_2T_x$ MXene

Hydrofluoric acid (HF) solutions was used to synthesize $Ti_3C_2T_x$ by etching Ti_3AlC_2 according to a previous literature [62]. Specifically, 1 g Ti_3AlC_2 (Forsman Scientific Co., Ltd) were immersed into 10 ml 40% HF solutions (Aladdin Co., Ltd) slowly, then the reaction mixture was held for 18 h at room temperature. After etching for 18 h, the mixture was washed through several cycles of distilled water addition by centrifugation, until the pH value of the supernatant reached approximately 6. The powders were then dispersed in the 50 ml TMAOH (Tetramethylammonium hydroxide 25 wt.% aqueous solution, J&K Scientific Co., Ltd.) and shook in the water bath shaker for 24 h at room temperature. Then the mixture was rinsed with for deionized water three times to remove residual TMAOH. Centrifugation for 30 min at 3500 rpm, the supernatants was separated from the sediment. The concentration of the supernatant was determined by lyophilizating a known volume of supernatant and measuring the weight of the powder.

2.2. Preparation of $MoS_2/Ti_3C_2T_x$ hybrid

The typical synthesis procedure of $MoS_2/Ti_3C_2T_x$ hybrid is as follows: 50 mg ammonium tetrathiomolybdate (ATM) was add to 5 ml the supernatant of $Ti_3C_2T_x$ (1 mg/ml), and sonicated 10 min for homogeneous mixing. After the ultra-sonication, the mixture was immersed immediately into the liquid nitrogen and freeze-dried in lyophilizer. The resulting product was annealed at 350 °C for 1 h under a mixture gas of argon and hydrogen (80%/20%) atmosphere with a heating rate of 5 °C/min.

2.3. Preparation of pure MoS_2

The preparation of MoS_2 was similar with the $MoS_2/Ti_3C_2T_x$ hybrid without the introduction the $Ti_3C_2T_x$.

2.4. Electrode preparation and electrochemical measurements

All the electrochemical measurements were carried out at ambient temperature in a standard three-electrode electrochemical cell with an electrochemical station (CHI 660D electrochemical station) in 0.5 M H_2SO_4. An Ag/AgCl (saturated KCl-filled) electrode was used as reference electrode. A glassy carbon electrode (3 mm in diameter) was served as the support for the working electrode. A graphite rod was used as counter electrode. Typically, 4 mg of catalysts and 40 μl 0.5 wt.% Nafion solution were dispersed in the 1 ml water–ethanol solution with volume ratio of 4:1 by sonicating to generate a homogeneous ink. In short, 5 μl well-dispersed catalysts was pipetted onto the glassy carbon electrode surface and then dried at ambient temperature for measurements. Polarization curves were obtained by linear sweep voltammetry with scan rate of 5 mVs^{-1}. The long-term electrochemical stability tests were evaluated by continuous cycling at a scan rate of 100 mVs^{-1}. Electrochemical impedance spectroscopy was studied over a frequency sweeping 100 K to 0.1 Hz at overpotential of 100 mV with an amplitude of 5 mV AC impedance. All the potentials used in the paper here was converted to the reversible hydrogen electrode (RHE), based on the Nernst equation $E_{RHE} = E_{Ag/AgCl} + 0.059\,\text{pH} + E^{\theta}_{Ag/AgCl}$.

2.5. Characterization

Samples were characterized by SEM (Hitachi, S4800), TEM (JEOL, Jem-2100 F), XRD (Panalytical X'Pert Pro, Cu–Kα radiation), Raman (Horiba, LabRAM HR Evolution with 532 nm laser excitation), X-ray photoelectron spectroscopy (Thermo Scientific, ESCALAB 250 XI).

3. Results and discussion

The synthetic process of the "nanoroll" like $MoS_2/Ti_3C_2T_x$ hybrid is illustrated in the Scheme 1. In brief, $Ti_3C_2T_x$ nanosheets that prepared by etching and intercalating Ti_3AlC_2 with HF and organic base were homogeneously mixed with ammonium tetrathiomolybdate (ATM) solution. The obtained dispersion was quickly frozen by liquid nitrogen and then subjected to loyphilization. The final $MoS_2/Ti_3C_2T_x$ hybrid was obtained by annealing the dried ATM/$Ti_3C_2T_x$ mixture at H_2/Ar atmosphere. Scanning electron microscopy (SEM) reveals that the exfoliated $Ti_3C_2T_x$ nanosheets (Fig. 1a) tend to roll automatically after meeting liquid nitrogen (Figure S1a). Similar phenomenon was observed when the ATM precursor was added (Figure S1b-d). The rolling of the $Ti_3C_2T_x$ nanosheets should be attributed to the quick freezing-induced shrinking by liquid nitrogen, which causes a sudden change in the strain of the $Ti_3C_2T_x$ nanosheets. And, the presence of the adsorbed MoS_2's precursors on the surface of $Ti_3C_2T_x$ may further increase the local strain and facilitate the rolling. Noted that this "nanoroll" like structure did not change even after annealing at high temperatures, and abundant $MoS_2/Ti_3C_2T_x$ nanorolls with diameter of ~200 nm and length of sever microns are finally obtained (Fig. 1b–d). Given most the nanorolls have length over 20 microns, these nanorolls observed should be formed by the rolling of adjacent $Ti_3C_2T_x$ nanosheets during the quick freezing-induced shrinking process.

Transmission electron microscopy (TEM) images (Fig. 2a,b) of the $MoS_2/Ti_3C_2T_x$ hybrid show that abundant "bubbles" (the circular areas with much less contrast) are located on the surface or/and in the channel of the $Ti_3C_2T_x$ nanoroll. Dark-field TEM image of these nanoroll shows clear open ends (Fig. 2d). Corresponding elemental mapping (Fig. 2e–h) confirms the uniform distribution of Mo, S, Ti and C elements in/on the nanoroll. High resolution TEM (Fig. 2c) reveals that this interesting "bubble" like structure is formed by few-layered MoS_2 crystallites with vertically aligned edges. The interlayer distance of these MoS_2 crystallites ~0.672 nm, which is obviously larger than that of the bulk crystal (~0.62 nm) [20] and supported by X-ray diffraction (XRD) results (Figure S2). This interesting phenomenon may be explained by the formation and evaporation of abundant ice crystals during the frozen and lyophilization of the ATM/$Ti_3C_2T_x$ precursor, which will decompose to $MoS_2/Ti_3C_2T_x$ hybrid after annealing. Note

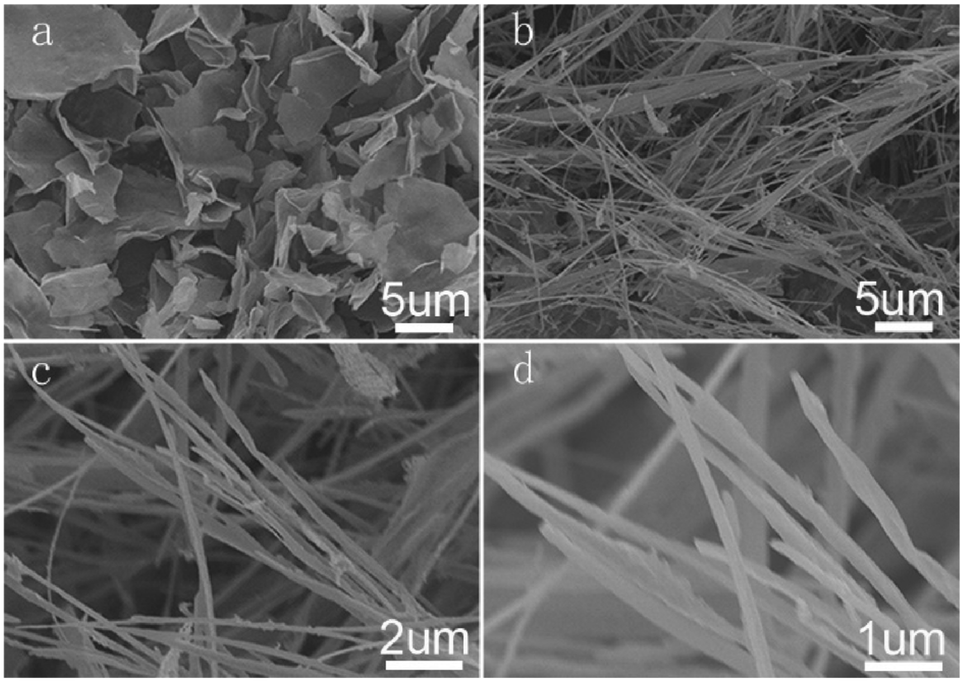

Fig. 1. (a) Representative SEM of the exfoliated $Ti_3C_2T_x$ nanosheets. (b–d) Typical SEM image of the "nanoroll" like $MoS_2/Ti_3C_2T_x$ hybrid under different magnifications.

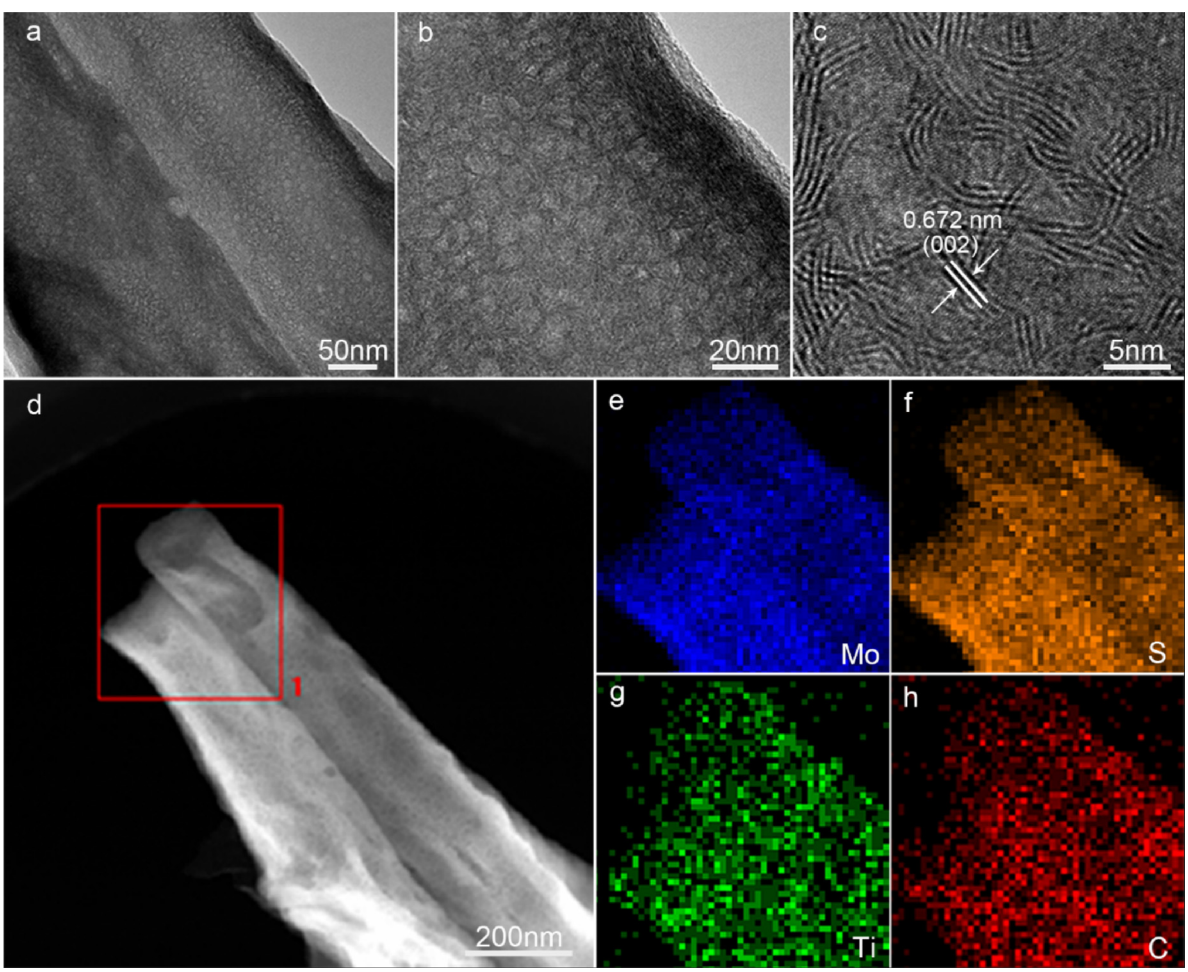

Fig. 2. (a–c) Representative TEM of the "nanoroll" like $MoS_2/Ti_3C_2T_x$ hybrid. (d–h) TEM images and corresponding EDX elemental mapping of Mo, S, Ti and C.

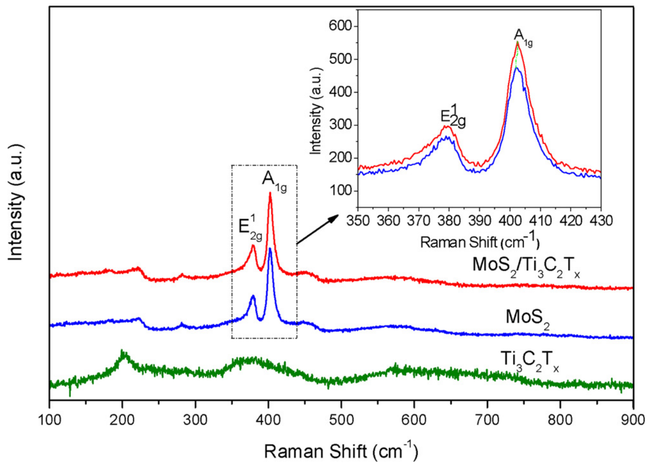

Fig. 3. Raman spectra of the $MoS_2/Ti_3C_2T_x$ hybrid, pure MoS_2 and $Ti_3C_2T_x$ nanosheets.

that these vertically aligned MoS_2 crystallites on the surface of $Ti_3C_2T_x$ may facilitate the mass diffusion and charge transfer process during electrocatalysis reactions, as the in-plane electron mobility of MoS_2 is about three orders of magnitude higher than the that perpendicular to the basal planes [17,26].

The Raman spectra of $Ti_3C_2T_x$ nanosheets, pure MoS_2 and $MoS_2/Ti_3C_2T_x$ hybrid are shown in Fig. 3. In line with previous studies [63–65], the Raman spectra of the exfoliated $Ti_3C_2T_x$ contains three broad peaks at approximately 202, 378 and 605 cm^{-1}. And, the weak broad peak at 605 cm^{-1} indicates that relatively fewer −OH groups are existed. The $MoS_2/Ti_3C_2T_x$ shows the characteristic in-plane (E^1_{2g}) and out-of-plane (A_{1g}) mode of MoS_2 at 379.2 and 402.5 cm^{-1}, respectively [15,66]. According to previous reports, the A_{1g} mode is the favored vibrational mode for edge-terminated structure [26–28,66,67]. Therefore, the decrease in the $I_{E^1_{2g}}/I_{A_{1g}}$ of the $MoS_2/Ti_3C_2T_x$ (compared with the MoS_2 control) indicates an edge-terminated structure for the vertically aligned MoS_2, in concert with the TEM observations. The slight blue-shift of the A_{1g} mode of MoS_2 in the $MoS_2/Ti_3C_2T_x$ hybrid should be caused by the increasing local strain of the MoS_2 [66].

The chemical states and surface chemical compositions of the examples were elucidated by X-ray photoelectron spectroscopy (XPS). From the survey scan of the $MoS_2/Ti_3C_2T_x$ (Figure S3), the concomitant of Mo, S, Ti and C elements were detected, in concert with TEM Mapping. The Mo 3d high-resolution spectra (Fig. 4) of the $MoS_2/Ti_3C_2T_x$ displays two main peaks at 229.1 and 232.1 eV, corresponding to the $3d_{5/2}$ and $3d_{3/2}$ doublet of Mo^{4+} components [66]. Note that these two peaks negatively shift by 0.2 eV when compared with the MoS_2 control, indicating the electron transfer from the $Ti_3C_2T_x$ to the MoS_2 in the hybrid [68]. This assumption is supported by the Ti 2p high-resolution spectra. As showed in Fig. 4, four doublets (Ti $2p_{3/2}$ and Ti $2p_{1/2}$) was used to fitted the core-level spectra. Note that the probe depth is only a few nm for XPS, and the signals originate solely from the surface of $MoS_2/Ti_3C_2T_x$ and $Ti_3C_2T_x$. Therefore, compared with the Ti 2p high-resolution of $Ti_3C_2T_x$ nanosheets, the Ti ions with a charge state of 4(TiO_2) obviously increased in the $MoS_2/Ti_3C_2T_x$ hybrid. In the meanwhile, the binding energy of the $2p_{3/2}$ orbit of Ti-C positively shift about 0.2 eV [69–71]. The strong interaction between MoS_2 and $Ti_3C_2T_x$, combining with the subsequent electron transfer should facilitate the charge transfer process during the electrocatalytic HER.

To verify this idea, the electrocatalytic HER performance of $MoS_2/Ti_3C_2T_x$ hybrid was systematically evaluated using a standard three-electrode system in 0.5 M H_2SO_4 solution (see details in the experimental section). For comparison, $Ti_3C_2T_x$, MoS_2 and 20% Pt/C were used as controls. Polarization curves after iR correction confirm that the $MoS_2/Ti_3C_2T_x$ hybrid shows much better HER activity than MoS_2, and $Ti_3C_2T_x$ is inner when the overpotential is less than 400 mV. In specific, the $MoS_2/Ti_3C_2T_x$ hybrid has an onset overpotential around 30 mV vs RHE, which is slightly higher than that of Pt/C catalyst, but that of the MoS_2 control is around 168 mV. To deliver the current density of 10 mA cm^{-2}, the $MoS_2/Ti_3C_2T_x$ hybrid needs an overpotential of 152 mV, while MoS_2 require a much larger overpotential of 337 mV. Note that the Tafel slope (Fig. 5b) of the Pt/C, $MoS_2/Ti_3C_2T_x$ hybrid, MoS_2 and $Ti_3C_2T_x$ are 30, 70, 101 and 162 mV dec^{-1}, respectively, suggesting the different mechanism involved. According to previous studies, for the $MoS_2/Ti_3C_2T_x$ hybrid, the Volmer-Heyrovsky mechanism should be the rate determining step, which refers to electrochemical-desorption of hydrogen [6]. To provide further insight into the catalytic performance of the $MoS_2/Ti_3C_2T_x$ hybrid, the exchange current density (j_0) was also calculated (Figure S4), and the results are summarized in Table 1. The exchange current of the $MoS_2/Ti_3C_2T_x$ hybrid and the MoS_2 control are determined to be 0.6165 mA cm^{-2} and 0.0239 mA cm^{-2}, respectively. This result indicates that a more than 25-fold increase in the exchange current density was observed. It should be noted that MoS_2 generally shows much lower exchange current densities than the precious metals, though it has a ΔG_H value near the optimum [11]. The > 25-fold increase of j_0 in the $MoS_2/Ti_3C_2T_x$ hybrid suggests that the significant increase in the absolute reaction rates.

To achieve further understanding for the electrode kinetics of the $MoS_2/Ti_3C_2T_x$ hybrid in the HER process, electrochemical impedance spectroscopy (EIS) was also performed. The Nyquist plots depicted in Fig. 5d reveal that $MoS_2/Ti_3C_2T_x$ hybrid has a much smaller charge-transfer resistance than pure MoS_2, owing to the fact that the $Ti_3C_2T_x$ has a small charge transfer resistance. According to the previous study on the MoS_2/carbon nanotubes [72,73] or MoS_2/graphene hybrids [5,74], the conductivity of the hybrids plays an important role in the electrocatalytic HER performances. Therefore, the introduced $Ti_3C_2T_x$ not only helps the dispersion of vertically aligned MoS_2, but also serves as an excellent conductive additive to facilitate the electron transfer from the substrate to the MoS_2.

Long-term stability is another crucial criterion for a good electrocatalyst. To assess the durability of the $MoS_2/Ti_3C_2T_x$ hybrid, a continuous cycling test was conducted at a 100 mVs^{-1} scan rate in 0.5 M H_2SO_4 solution. As shown in Fig. 5c, negligible decay of polarization curve can be noticed before and after 1000, 2000 and 3000 cycles. In addition, the durability of $MoS_2/Ti_3C_2T_x$ hybrid was also examined by electrolysis at a static overpotential of 152 mV. The inset of Fig. 5c shows that the current density experienced a negligible loss at ~10 mA cm^{-2} for 12 h. The negligible difference confirms the outstanding durability of the $MoS_2/Ti_3C_2T_x$ hybrid as electrocatalysts in HER. Noted that the “nanoroll” like structure did not change even after the electrochemical test (Figure S5).

4. Conclusion

In summary, we report a simple strategy for synthesizing the “nanoroll” like hierarchical structure $MoS_2/Ti_3C_2T_x$ hybrid by combining liquid nitrogen-freezing and subsequent annealing. We found that the quick freezing-process played a key role in the rolling of $Ti_3C_2T_x$ nanosheets and the formation of vertically aligned MoS_2 crystallites. This unique hierarchical architecture of the $MoS_2/Ti_3C_2T_x$ hybrid affords more active sites and facilitate the charge transfer process during electrocatalysis reaction. Therefore, it shows excellent HER catalytic activity with a small onset overpotential of 30 mV. In addition, a more than 25-fold increase in the exchange current density compared with MoS_2 was also observed. The methods described here may be applicable to the preparation of other MXene-based hybrids with novel hierarchical structures for a variety of applications.

Acknowledgments

This study is supported by the National Natural Science Funds (No.

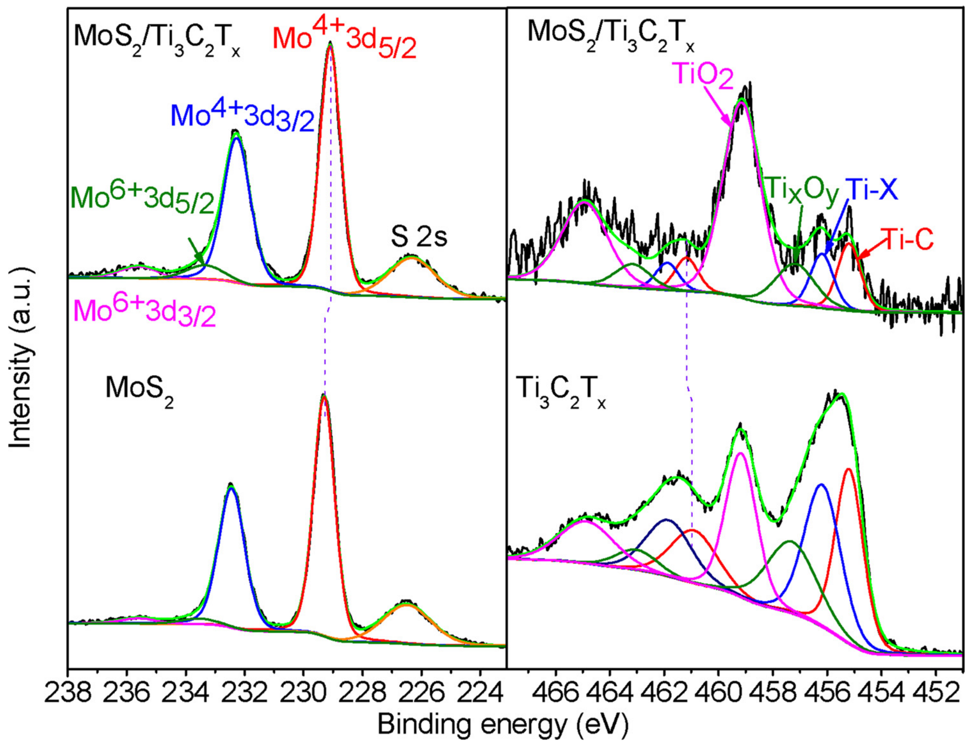

Fig. 4. Mo 3d and S 2 s XPS spectra of $MoS_2/Ti_3C_2T_x$ hybrid; Ti 2p high-resolution XPS spectra of $MoS_2/Ti_3C_2T_x$ hybrid; Mo 3d and S 2 s XPS spectra of MoS_2; Ti 2p high-resolution XPS spectra of $Ti_3C_2T_x$ nanosheets.

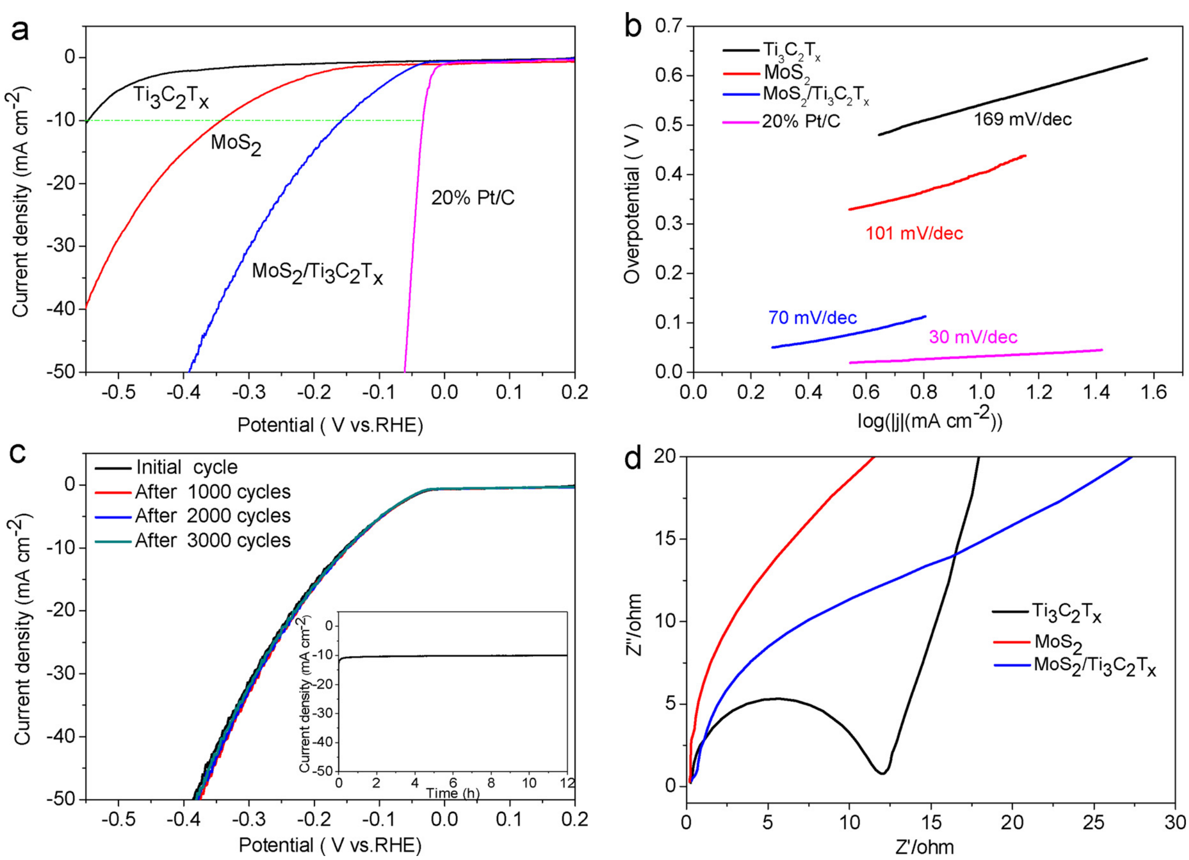

Fig. 5. a) Polarization curves and (b) Tafel plots of $MoS_2/Ti_3C_2T_x$ hybrid, pure MoS_2 and $Ti_3C_2T_x$ nanosheets. (c) Polarization curves were recorded for $MoS_2/Ti_3C_2T_x$ hybrid before and after 1000, 2000 and 3000 potential cycles, respectively. Inset: Time-dependent current density curve of $MoS_2/Ti_3C_2T_x$ hybrid under a static overpotential of 152 mV for 12 h. (d) Electrochemical impedance spectroscopy of $MoS_2/Ti_3C_2T_x$ hybrid, pure MoS_2 and $Ti_3C_2T_x$ nanosheets at overpotential of 100 mV.

Table 1
Comparison of catalytic parameters of different HER[a] catalysts.

Catalyst[b]	Onset potential (mV vs RHE[c])	J_o[d] (mA cm^{-2})
MoS_2	168	0.0239
$MoS_2/Ti_3C_2T_x$	30	0.6165

[a] HER, H_2 evolution reaction.
[b] All the parameters were measured under the same conditions.
[c] RHE, reversible hydrogen electrode.
[d] Exchange current densities(J_o) were obtained from Tafel curves by using extrapolation method.

21676198) and the Program of Introducing Talents of Discipline to Universities (No. B06006).

Appendix A. Supplementary data

Supplementary material related to this article can be found, in the online version, at doi:https://doi.org/10.1016/j.apcatb.2018.08.083.

References

[1] M. Caban-Acevedo, M.L. Stone, J.R. Schmidt, J.G. Thomas, Q. Ding, H.C. Chang, M.L. Tsai, J.H. He, S. Jin, Nat. Mater. 14 (2015) 1245–1251.
[2] R. Ye, P. del Angel-Vicente, Y. Liu, M.J. Arellano-Jimenez, Z. Peng, T. Wang, Y. Li, B.I. Yakobson, S.H. Wei, M.J. Yacaman, J.M. Tour, Adv. Mater. 28 (2016) 1427–1432.
[3] Y. Zheng, Y. Jiao, Y. Zhu, L.H. Li, Y. Han, Y. Chen, A. Du, M. Jaroniec, S.Z. Qiao, Nat. Commun. 5 (2014) 3783.
[4] X. Fan, Y. Liu, Z. Peng, Z. Zhang, H. Zhou, X. Zhang, B.I. Yakobson, W.A. Goddard 3rd, X. Guo, R.H. Hauge, J.M. Tour, ACS Nano 11 (2017) 384–394.
[5] Y. Li, H. Wang, L. Xie, Y. Liang, G. Hong, H. Dai, J. Am. Chem. Soc. 133 (2011) 7296–7299.
[6] J. Xie, H. Zhang, S. Li, R. Wang, X. Sun, M. Zhou, J. Zhou, X.W. Lou, Y. Xie, Adv. Mater. 25 (2013) 5807–5813.
[7] Z. Chen, K. Leng, X. Zhao, S. Malkhandi, W. Tang, B. Tian, L. Dong, L. Zheng, M. Lin, B.S. Yeo, K.P. Loh, Nat. Commun. 8 (2017) 14548.
[8] J. Mahmood, F. Li, S.M. Jung, M.S. Okyay, I. Ahmad, S.J. Kim, N. Park, H.Y. Jeong, J.B. Baek, Nat. Nanotechnol. 12 (2017) 441–446.
[9] Y. Chen, G. Yu, W. Chen, Y. Liu, G.D. Li, P. Zhu, Q. Tao, Q. Li, J. Liu, X. Shen, H. Li, X. Huang, D. Wang, T. Asefa, X. Zou, J. Am. Chem. Soc. 139 (2017) 12370–12373.
[10] A. Travert, H. Nakamura, R.A. van Santen, S. Cristol, J.F. Paul, E. Payen, J. Am. Chem. Soc. 124 (2002) 7084–7095.
[11] T.F. Jaramillo, K.P. Jorgensen, J. Bonde, J.H. Nielsen, S. Horch, I. Chorkendorff, Science 317 (2007) 100–102.
[12] H. Li, C. Tsai, A.L. Koh, L. Cai, A.W. Contryman, A.H. Fragapane, J. Zhao, H.S. Han, H.C. Manoharan, F. Abild-Pedersen, J.K. Norskov, X. Zheng, Nat. Mater. 15 (2016) 48–53.
[13] C. Tsai, K.R. Chan, J.K. Norskov, F. Abild-Pedersen, Surf. Sci. 640 (2015) 133–140.
[14] G. Li, D. Zhang, Q. Qiao, Y. Yu, D. Peterson, A. Zafar, R. Kumar, S. Curtarolo, F. Hunte, S. Shannon, Y. Zhu, W. Yang, L. Cao, J. Am. Chem. Soc. 138 (2016) 16632–16638.
[15] Y. Yin, J. Han, Y. Zhang, X. Zhang, P. Xu, Q. Yuan, L. Samad, X. Wang, Y. Wang, Z. Zhang, P. Zhang, X. Cao, B. Song, S. Jin, J. Am. Chem. Soc. 138 (2016) 7965–7972.
[16] J. Chen, X.J. Wu, Y. Gong, Y. Zhu, Z. Yang, B. Li, Q. Lu, Y. Yu, S. Han, Z. Zhang, Y. Zong, Y. Han, L. Gu, H. Zhang, J. Am. Chem. Soc. 139 (2017) 8653–8660.
[17] J. Hu, B.L. Huang, C.X. Zhang, Z.L. Wang, Y.M. An, D. Zhou, H. Lin, M.K.H. Leung, S.H. Yang, Energy Environ. Sci. 10 (2017) 593–603.
[18] Z. Lin, B.R. Carvalho, E. Kahn, R. Lv, R. Rao, H. Terrones, M.A. Pimenta, M. Terrones, 2D Mater. 3 (2016).
[19] H. Zhang, R. Lv, J. Mater. 4 (2) (2018) 95–107.
[20] X. Fan, P. Xu, Y.C. Li, D. Zhou, Y. Sun, M.A. Nguyen, M. Terrones, T.E. Mallouk, J. Am. Chem. Soc. 138 (2016) 5143–5149.
[21] X. Fan, P. Xu, D. Zhou, Y. Sun, Y.C. Li, M.A. Nguyen, M. Terrones, T.E. Mallouk, Nano Lett. 15 (2015) 5956–5960.
[22] X. Hai, K. Chang, H. Pang, M. Li, P. Li, H. Liu, L. Shi, J. Ye, J. Am. Chem. Soc. 138 (2016) 14962–14969.
[23] K.R. Paton, E. Varrla, C. Backes, R.J. Smith, U. Khan, A. O'Neill, C. Boland, M. Lotya, O.M. Istrate, P. King, T. Higgins, S. Barwich, P. May, P. Puczkarski, I. Ahmed, M. Moebius, H. Pettersson, E. Long, J. Coelho, S.E. O'Brien, E.K. McGuire, B.M. Sanchez, G.S. Duesberg, N. McEvoy, T.J. Pennycook, C. Downing, A. Crossley, V. Nicolosi, J.N. Coleman, Nat. Mater. 13 (2014) 624–630.
[24] J. Kibsgaard, Z. Chen, B.N. Reinecke, T.F. Jaramillo, Nat. Mater. 11 (2012) 963–969.
[25] J. Deng, H. Li, S. Wang, D. Ding, M. Chen, C. Liu, Z. Tian, K.S. Novoselov, C. Ma, D. Deng, X. Bao, Nat. Commun. 8 (2017) 14430.
[26] S.M. Tan, A. Ambrosi, Z. Sofer, S. Huber, D. Sedmidubsky, M. Pumera, Chemistry 21 (2015) 7170–7178.
[27] Y. Yang, H. Fei, G. Ruan, C. Xiang, J.M. Tour, Adv. Mater. 26 (2014) 8163–8168.
[28] Y. Sun, F. Alimohammadi, D. Zhang, G. Guo, Nano Lett. 17 (2017) 1963–1969.
[29] D. Voiry, R. Fullon, J. Yang, E.S.C. de Carvalho Castro, R. Kappera, I. Bozkurt, D. Kaplan, M.J. Lagos, P.E. Batson, G. Gupta, A.D. Mohite, L. Dong, D. Er, V.B. Shenoy, T. Asefa, M. Chhowalla, Nat. Mater. 15 (2016) 1003–1009.
[30] D. Voiry, M. Salehi, R. Silva, T. Fujita, M. Chen, T. Asefa, V.B. Shenoy, G. Eda, M. Chhowalla, Nano Lett. 13 (2013) 6222–6227.
[31] M.A. Worsley, S.J. Shin, M.D. Merrill, J. Lenhardt, A.J. Nelson, L.Y. Woo, A.E. Gash, T.F. Baumann, C.A. Orme, ACS Nano 9 (2015) 4698–4705.
[32] K. Chang, Z. Mei, T. Wang, Q. Kang, S. Ouyang, J. Ye, ACS Nano 8 (2014) 7078–7087.
[33] L. Liao, J. Zhu, X. Bian, L. Zhu, M.D. Scanlon, H.H. Girault, B. Liu, Adv. Funct. Mater. 23 (2013) 5326–5333.
[34] Z. Zhao, F. Qin, S. Kasiraju, L. Xie, M.K. Alam, S. Chen, D. Wang, Z. Ren, Z. Wang, L.C. Grabow, J. Bao, ACS Catal. 7 (2017) 7312–7318.
[35] X. Han, X. Tong, X. Liu, A. Chen, X. Wen, N. Yang, X.-Y. Guo, ACS Catal. 8 (2018) 1828–1836.
[36] B. Anasori, M.R. Lukatskaya, Y. Gogotsi, Nat. Rev. Mater. 2 (2017).
[37] M.R. Lukatskaya, O. Mashtalir, C.E. Ren, Y. Dall'Agnese, P. Rozier, P.L. Taberna, M. Naguib, P. Simon, M.W. Barsoum, Y. Gogotsi, Science 341 (2013) 1502–1505.
[38] M. Ghidiu, M.R. Lukatskaya, M.Q. Zhao, Y. Gogotsi, M.W. Barsoum, Nature 516 (2014) 78–81.
[39] O. Mashtalir, M. Naguib, V.N. Mochalin, Y. Dall'Agnese, M. Heon, M.W. Barsoum, Y. Gogotsi, Nat. Commun. 4 (2013) 1716.
[40] A. Lipatov, M. Alhabeb, M.R. Lukatskaya, A. Boson, Y. Gogotsi, A. Sinitskii, Adv. Electron. Mater. 2 (2016) 1600255.
[41] G. Gao, A.P. O'Mullane, A. Du, ACS Catal. 7 (2016) 494–500.
[42] J. Luo, X. Tao, J. Zhang, Y. Xia, H. Huang, L. Zhang, Y. Gan, C. Liang, W. Zhang, ACS Nano 10 (2016) 2491.
[43] S.J. Kim, H.J. Koh, C.E. Ren, O. Kwon, K. Maleski, S.Y. Cho, B. Anasori, C.K. Kim, Y.K. Choi, J. Kim, ACS Nano 12 (2) (2018) 986–993.
[44] Z. Wang, J. Xuan, Z. Zhao, Q. Li, F. Geng, ACS Nano 11 (2017).
[45] M. Hu, T. Hu, Z. Li, Y. Yang, R. Cheng, J. Yang, C. Cui, X. Wang, ACS Nano 12 (4) (2018) 3578–3586.
[46] M. Ming, Y. Ren, M. Hu, Y. Zhang, T. Sun, Y. Ma, X. Li, W. Jiang, D. Gao, J. Bi, G. Fan, Appl. Catal. B: Environ. 210 (2017) 462–469.
[47] X. Xie, N. Zhang, Z.-R. Tang, M. Anpo, Y.-J. Xu, Appl. Catal. B: Environ. 237 (2018) 43–49.
[48] H. Wang, Y. Wu, T. Xiao, X. Yuan, G. Zeng, W. Tu, S. Wu, H.Y. Lee, Y.Z. Tan, J.W. Chew, Appl. Catal. B: Environ. 233 (2018) 213–225.
[49] T.Y. Ma, J.L. Cao, M. Jaroniec, S.Z. Qiao, Angew. Chem. Int. Ed. Engl. 55 (2016) 1138–1142.
[50] M. Yu, S. Zhou, Z. Wang, J. Zhao, J. Qiu, Nano Energy 44 (2018) 181–190.
[51] S. Zhou, X. Yang, W. Pei, N. Liu, J. Zhao, Nanoscale 10 (2018) 10876–10883.
[52] P. Li, J. Zhu, A.D. Handoko, R. Zhang, H. Wang, D. Legut, X. Wen, Z. Fu, Z.W. Seh, Q. Zhang, J. Mater. Chem. A 6 (2018) 4271–4278.
[53] Z. Guo, J. Zhou, Z. Sun, J. Mater. Chem. A 5 (2017) 23530–23535.
[54] C. Ling, L. Shi, Y. Ouyang, J. Wang, Chem. Mater. 28 (2016) 9026–9032.
[55] C. Ling, L. Shi, Y. Ouyang, Q. Chen, J. Wang, Adv. Sci. (Weinh) 3 (2016) 1600180.
[56] Z.W. Seh, K.D. Fredrickson, B. Anasori, J. Kibsgaard, A.L. Strickler, M.R. Lukatskaya, Y. Gogotsi, T.F. Jaramillo, A. Vojvodic, ACS Energy Lett. 1 (2016) 589–594.
[57] M. Pandey, K.S. Thygesen, J. Phys. Chem. C 121 (2017) 13593–13598.
[58] H. Pan, Sci. Rep. 6 (2016) 32531.
[59] S. Li, P. Tuo, J. Xie, X. Zhang, J. Xu, J. Bao, B. Pan, Y. Xie, Nano Energy 47 (2018) 512–518.
[60] W. Jiang, X. Zou, H. Du, L. Gan, C. Xu, F. Kang, W. Duan, J. Li, Chem. Mater. 30 (2018) 2687–2693.
[61] X. Wu, Z. Wang, M. Yu, L. Xiu, J. Qiu, Adv. Mater. 29 (2017).
[62] J. Xuan, Z. Wang, Y. Chen, D. Liang, L. Cheng, X. Yang, Z. Liu, R. Ma, T. Sasaki, F. Geng, Angew. Chem. Int. Ed. Engl. 55 (2016) 14569–14574.
[63] Y. Tang, J. Zhu, C. Yang, F. Wang, J. Electrochem. Soc. 163 (2016) A1975–A1982.
[64] M. Han, X. Yin, X. Li, B. Anasori, L. Zhang, L. Cheng, Y. Gogotsi, ACS Appl. Mater. Interfaces 9 (2017) 20038–20045.
[65] M. Naguib, O. Mashtalir, M.R. Lukatskaya, B. Dyatkin, C. Zhang, V. Presser, Y. Gogotsi, M.W. Barsoum, Chem. Commun. (Camb.) 50 (2014) 7420–7423.
[66] P.S. Toth, M. Velicky, M.A. Bissett, T.J. Slater, N. Savjani, A.K. Rabiu, A.M. Rakowski, J.R. Brent, S.J. Haigh, P. O'Brien, R.A. Dryfe, Adv. Mater. 28 (2016) 8256–8264.
[67] D. Kong, H. Wang, J.J. Cha, M. Pasta, K.J. Koski, J. Yao, Y. Cui, Nano Lett. 13 (2013) 1341–1347.
[68] Y. Shi, J. Wang, C. Wang, T.T. Zhai, W.J. Bao, J.J. Xu, X.H. Xia, H.Y. Chen, J. Am. Chem. Soc. 137 (2015) 7365–7370.
[69] R.B. Rakhi, B. Ahmed, M.N. Hedhili, D.H. Anjum, H.N. Alshareef, Chem. Mater. 27 (2015) 5314–5323.
[70] Y. Dall'Agnese, M.R. Lukatskaya, K.M. Cook, P.L. Taberna, Y. Gogotsi, P. Simon, Electrochem. Commun. 48 (2014) 118–122.
[71] C. Peng, X. Yang, Y. Li, H. Yu, H. Wang, F. Peng, ACS Appl. Mater. Interfaces 8 (2016) 6051–6060.
[72] H. Huang, W. Huang, Z. Yang, J. Huang, J. Lin, W. Liu, Y. Liu, J. Mater. Chem. A 5 (2016).
[73] P. Li, Z. Yang, J.X. Shen, H.G. Nie, Q.R. Cai, L.H. Li, M.Z. Ge, C.C. Gu, X. Chen, K.Q. Yang, L.J. Zhang, Y. Chen, S.M. Huang, ACS Appl. Mater. Interfaces 8 (2016) 3543–3550.
[74] L. Ma, Y. Hu, G. Zhu, R. Chen, T. Chen, H. Lu, Y. Wang, J. Liang, H. Liu, C. Yan, Chem. Mater. 28 (2016).